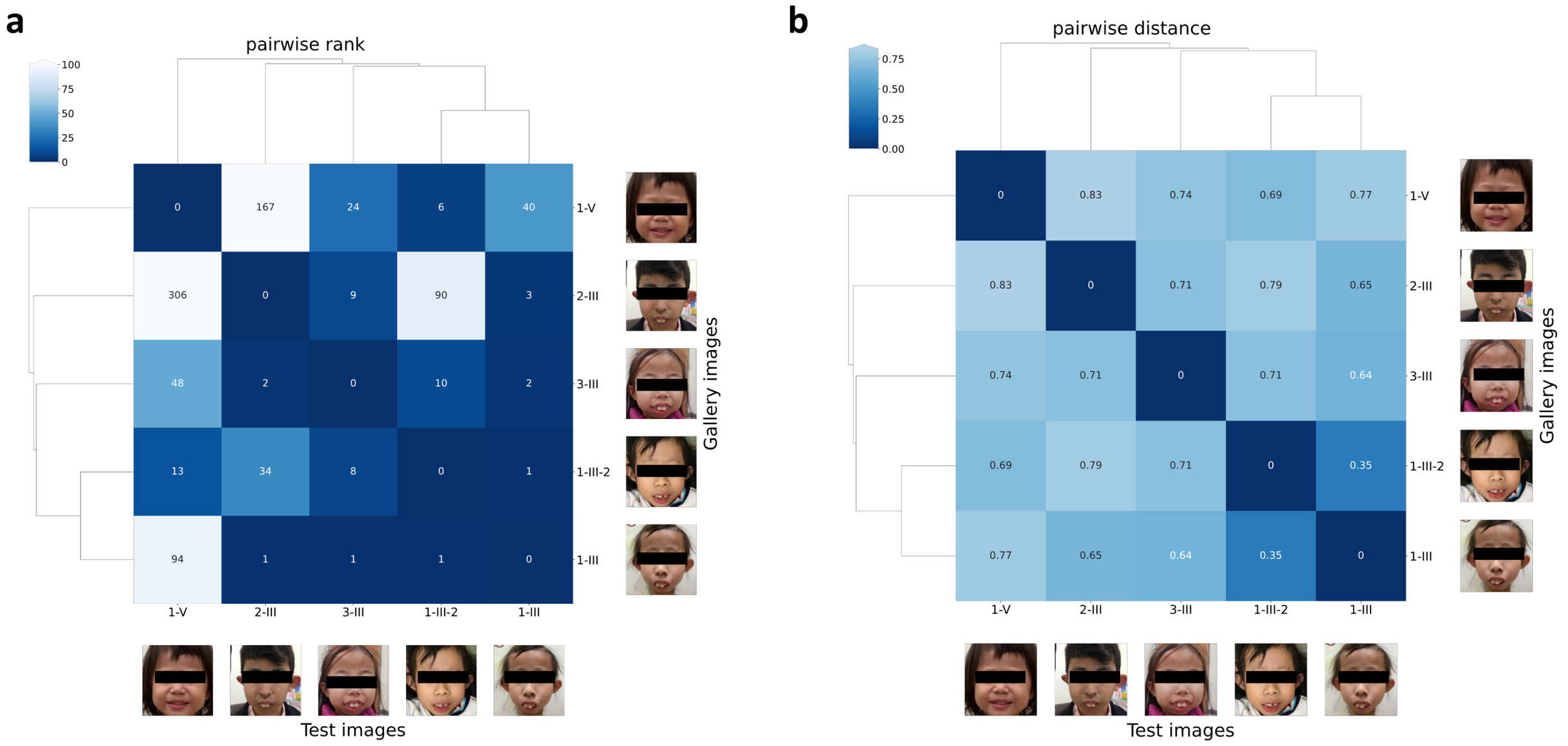

Figure S1. **Analysis of facial similarity among the patients.** (**a**) Pairwise rank matrix and hierarchical clustering of the five images. Each column represented the result of the rank of the rest four images in each row when analyzing one image in the column. The smaller the rank was, the closer the two images were in the phenotype space, and the more similar the two images were. For example, by testing image 1-III, image 1-III-2 was on the 1st rank, and 3-III was on the 2nd rank. Images 1-III (10-years-old) and 1-III-2 (5-years-old) were taken from the same patient 1-III at different ages. Patients 1-III and 1-V are family members. (**b**) Pairwise distance matrix and hierarchical clustering of the five images. Each cell represented the cosine distance between two images. The smaller the distance was, the closer the two images were in the phenotype space and the more similar the two images were. For example, 3-III was more similar to 1-III than to 1-III-2, because the distance of 0.64 was smaller than 0.71. Images 1-III (10-years-old) and 1-III-2 (5-years-old) were taken from the same proband 1-III at different ages. Patients 1-III and 1-V are family members.

Figure S2. Clinical features of patients with *TOMM7* p.P29L variant. (**a**) Dystrophic nails of the probands. (**b**) Fundus photography showing macular scars of the 2-year-old patient 1-V. (**c**) Whole body bone X-ray of proband 3-III.

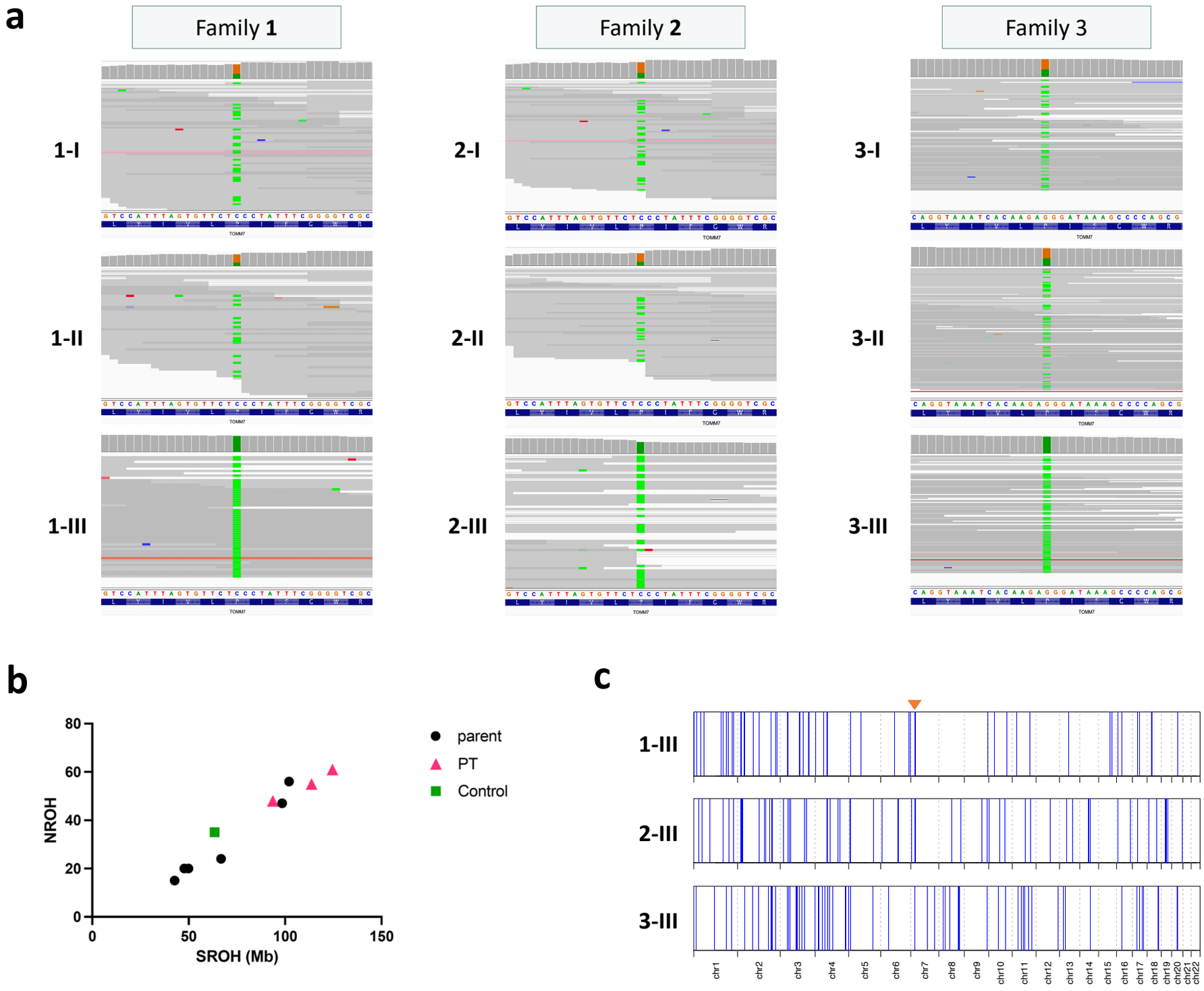

Figure S3. Recurrent *TOMM7* p.P29L variant in three unrelated families. (**a**) Representative IGV image of NGS showing homozygous missense variant of *TOMM7* in patients and heterozygous in their parents. (**b**) The total sum of runs of homozygosity (SROH) and the number of runs of homozygosity (NROH) were calculated from exome sequencing results of the family members (parents in black dot, probands in red triangle) and an unrelated control (green square). (**c**) Runs of homozygosity (ROH) with exome sequencing data showing genomic regions with ROH spanning over one million bases (blue lines). *TOMM7* is located in the shared ROH on chromosome 7 among patients (orange triangle).

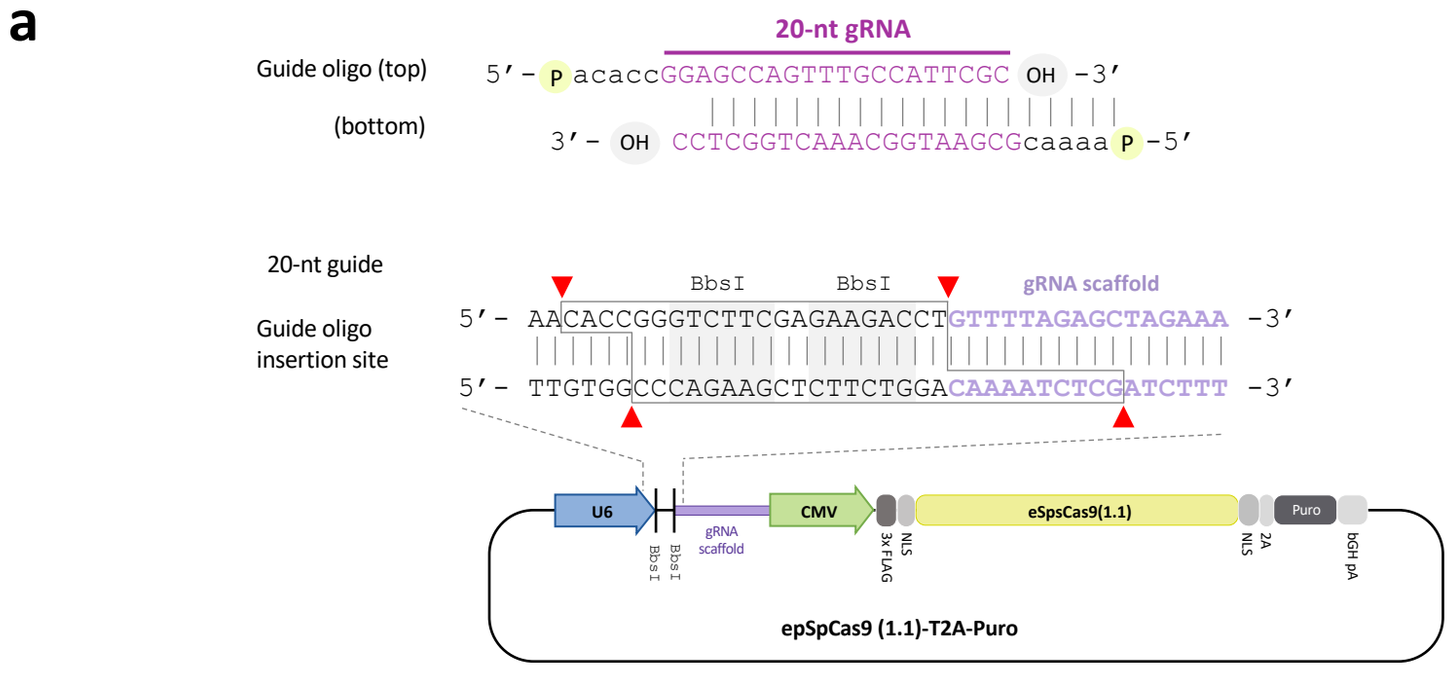

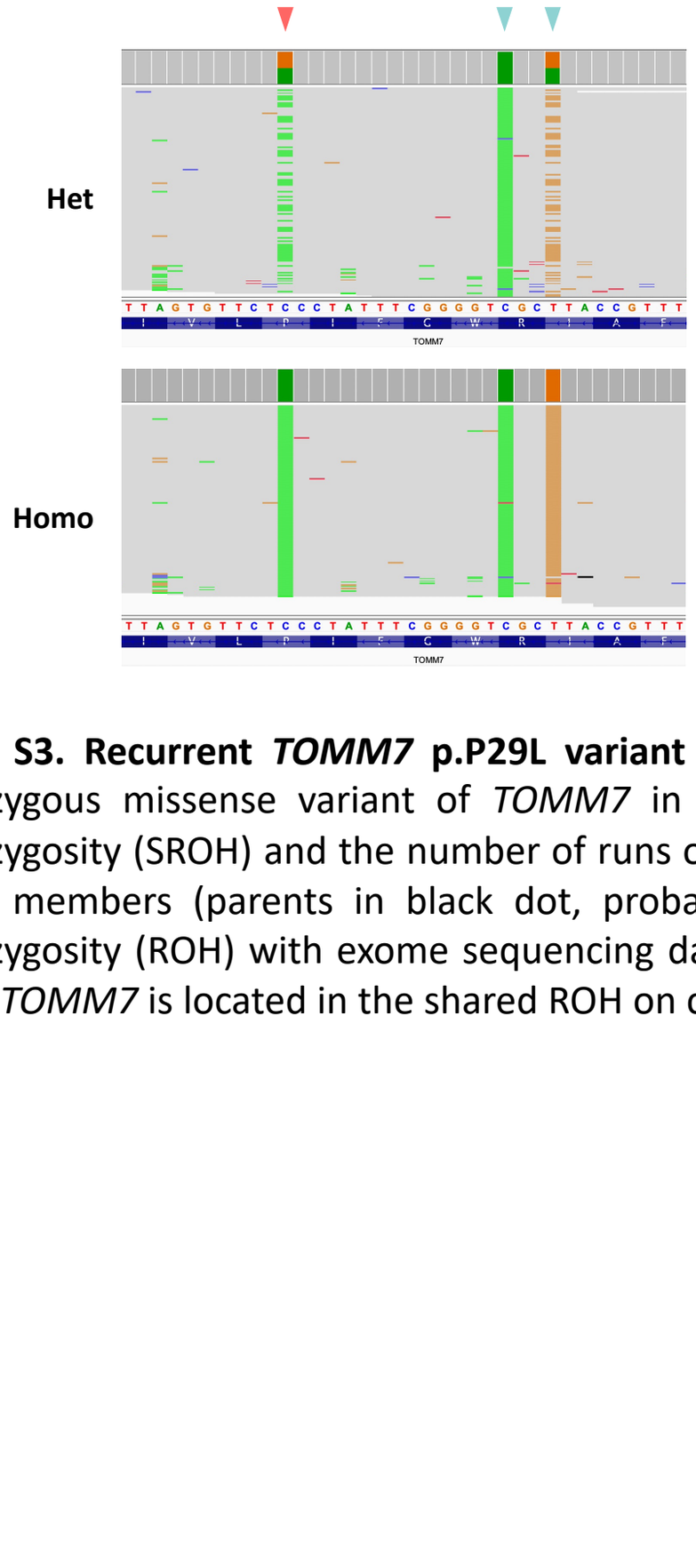

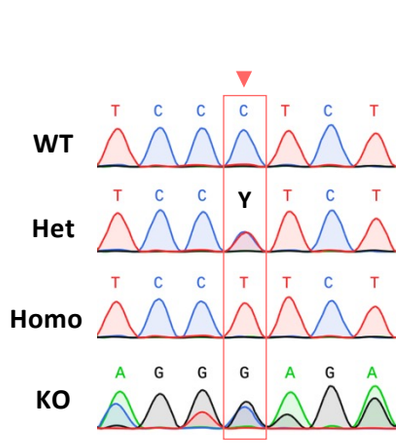

Figure S3. Recurrent *TOMM7* p.P29L variant in three unrelated families. (**a**) Representative IGV image of NGS showing homozygous missense variant of *TOMM7* in patients and heterozygous in their parents. (**b**) The total sum of runs of homozygosity (SROH) and the number of runs of homozygosity (NROH) were calculated from exome sequencing results of the family members (parents in black dot, probands in red triangle) and an unrelated control (green square). (**c**) Runs of homozygosity (ROH) with exome sequencing data showing genomic regions with ROH spanning over one million bases (blue lines). *TOMM7* is located in the shared ROH on chromosome 7 among patients (orange triangle).

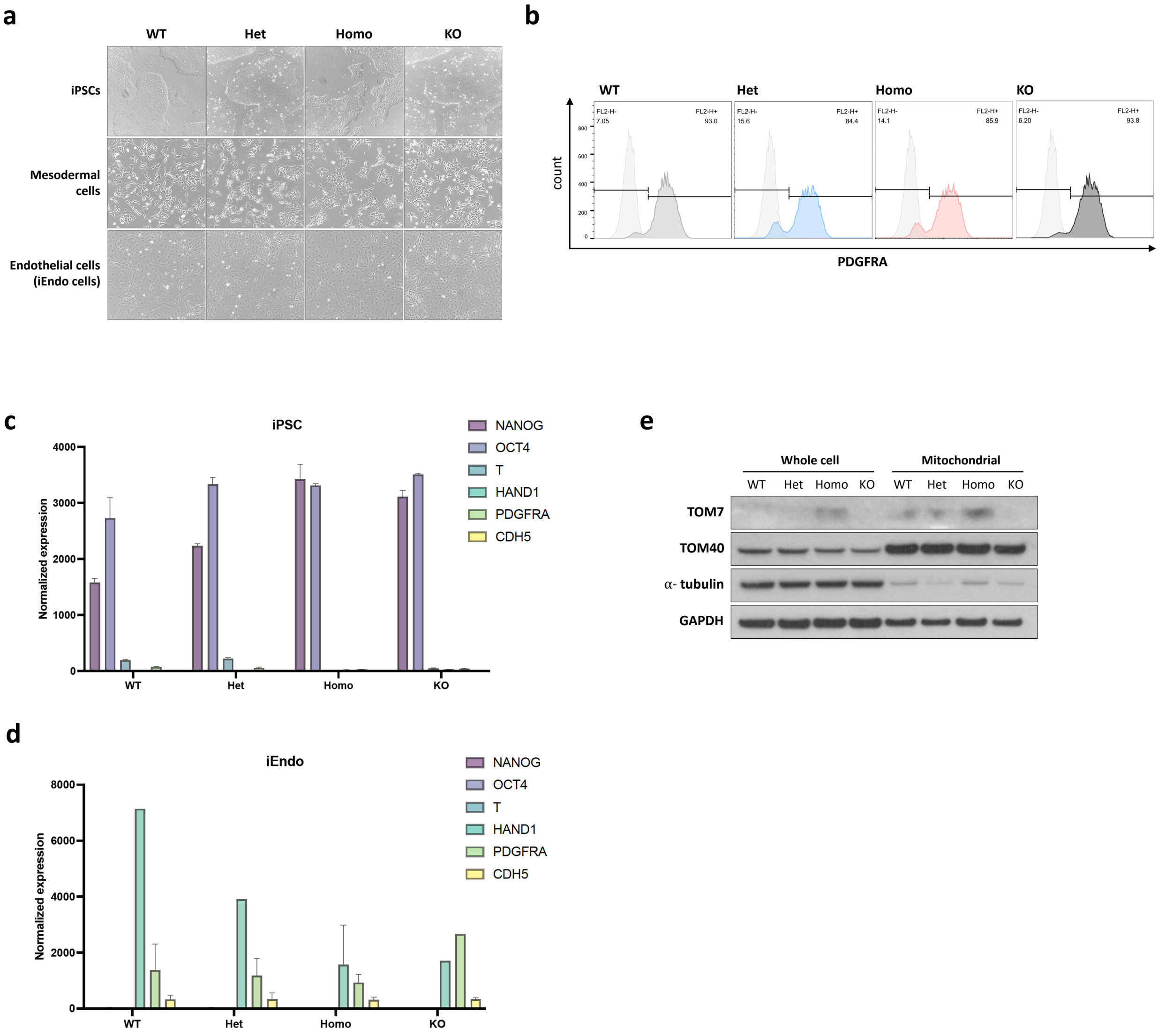

Figure S5. Differentiation and functional assays in CRISPR-edited iPSCs-derived endothelial cell. (**a**) Cell morphology of iPSCs, iPSC-derived mesodermal cells and iPSC-derived endothelial (iEndo) cells. (**b**) Representative flow cytometry for PDGFRA-positive cells on day 2 of differentiation. (**c and d**) Results from RNAseq showing read count of markers for iPSCs (*NANOG* and *OCT4*), mesodermal cells (*T*, *HAND1*, and *PDGFRA*) and endothelial cells (*HAND1*, *PDGFRA* and *CDH5*) in iPSCs (b) and iEndo cells (c). (**e**) Immunoblotting with anti-TOM7 and anti-TOM40 antibodies in whole-cell lysate and in mitochondria-enriched lysates from iEndo cells. WT, wild-type; Het, heterozygous *TOMM7*$^{+/PL}$; Homo, homozygous *TOMM7*$^{PL/PL}$; KO, *TOMM7* knock-out *TOMM7*$^{-/-}$. Data were presented as mean ± S.E.M.

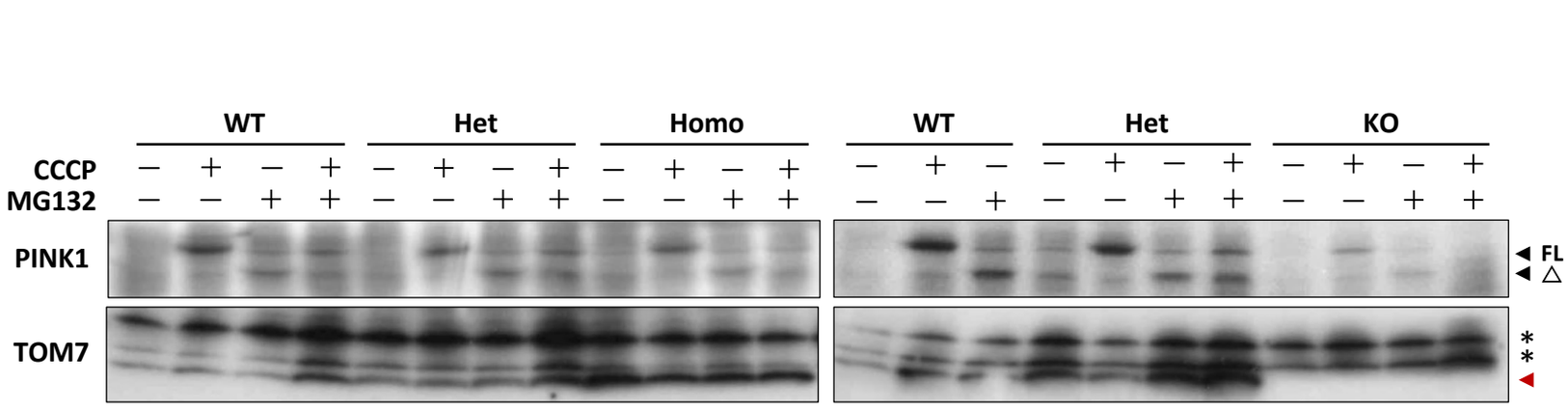

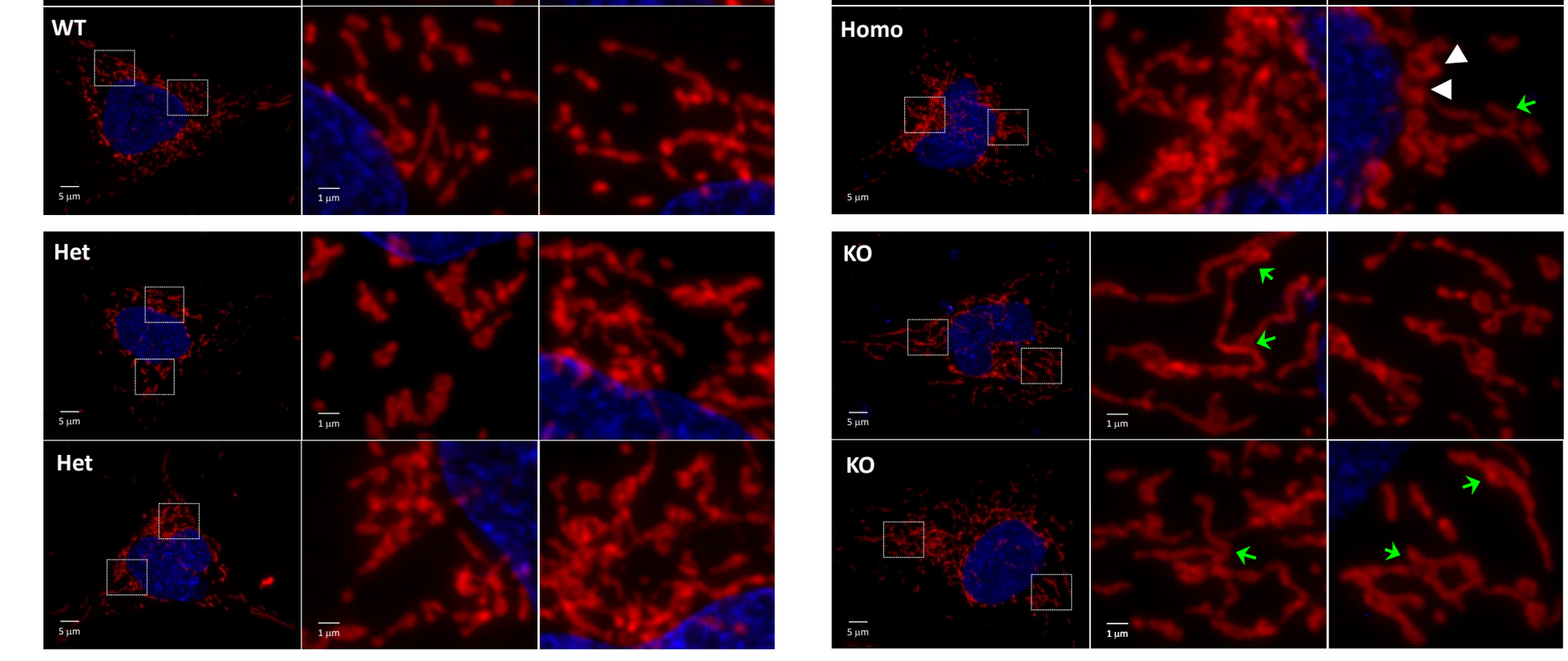

Figure S6. Mitochondrial quality control and functional assays in iPSC-derived endothelial cells with *TOMM7* variant. (**a**) Initiation of mitochondrial mitophagy monitored by the accumulation of full-length PINK1 precursor. The cleaved form of PINK1 was detected with the treatment of proteasome inhibitor MG132. iEndo cells were treated with 20 mM CCCP and/or 10mM MG132 for 6 hr and lyzed for immunoblotting. FL, full-length; Δ, cleaved. *, non-specific bands; red triangle, TOM7. (**b**) Quantification of full-length PINK1 in iEndo cells in (a). (**c**) Extension data of Figure 3e. Representative confocal images of immunofluorescent staining with anti-TOM40 (Red; staining mitochondria) and DAPI in iEndo cells. White arrowheads indicate large, round mitochondria. Green arrows indicate elongated mitochondria. (**d**) Tracing of Complex I activity and Complex III activity at 30-sec intervals for 10 min in iEndo cells. (**e**) NAD^+/NADH level in iEndo cells. (**f**) Quantification of the staining of MitoSOX in iEndo cells by flow cytometry. WT, wild-type; Het, heterozygous *TOMM7*$^{+/PL}$; Homo, homozygous *TOMM7*$^{PL/PL}$; KO, *TOMM7* knock-out. Data were presented as mean ± S.E.M. *P < 0.05, **P < 0.01 , ***P < 0.001.

a

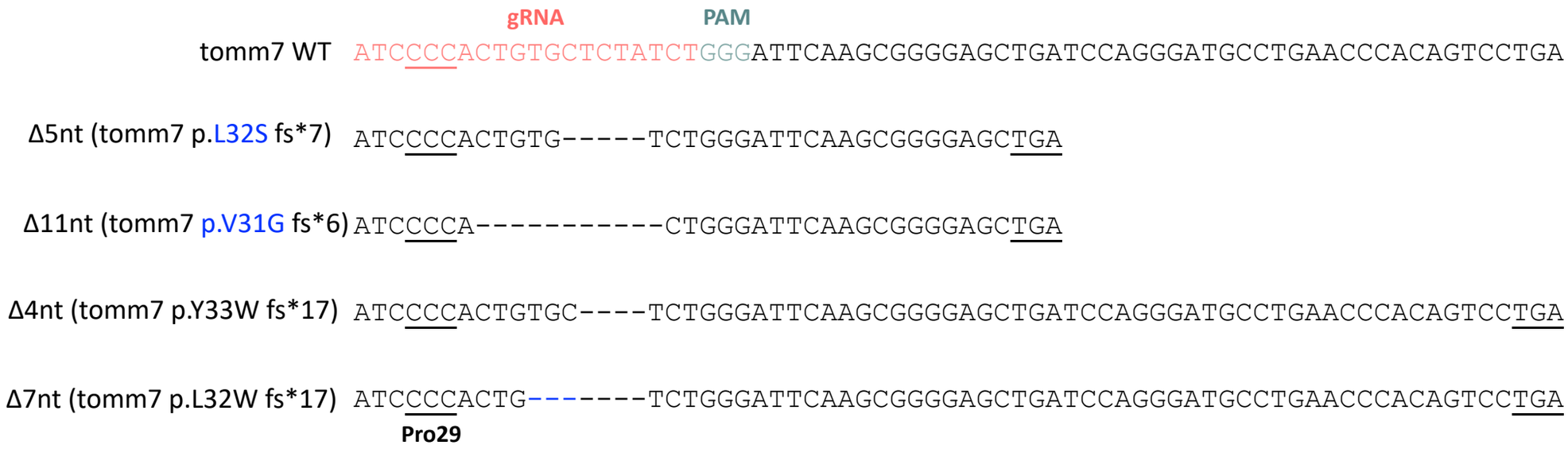

b

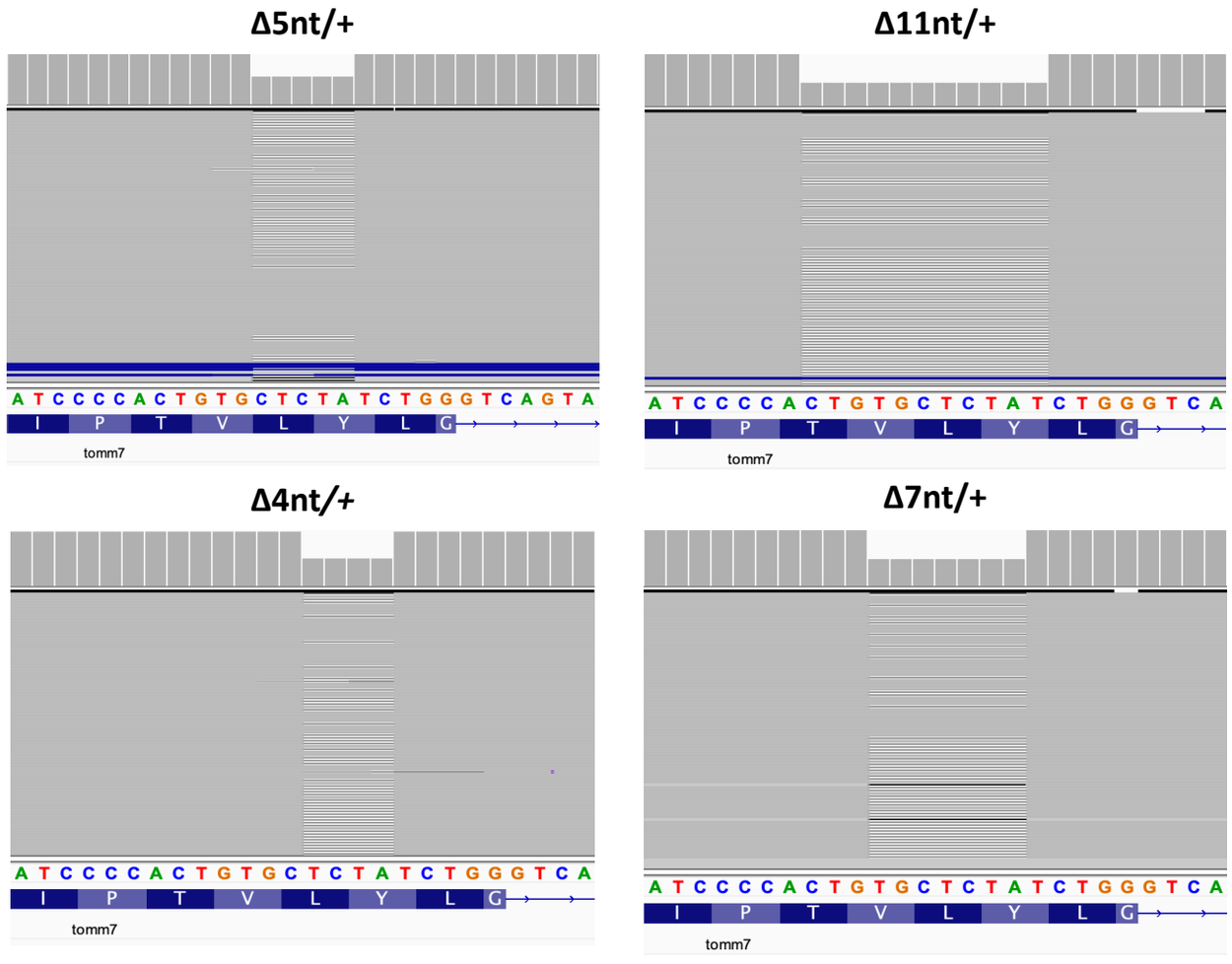

c

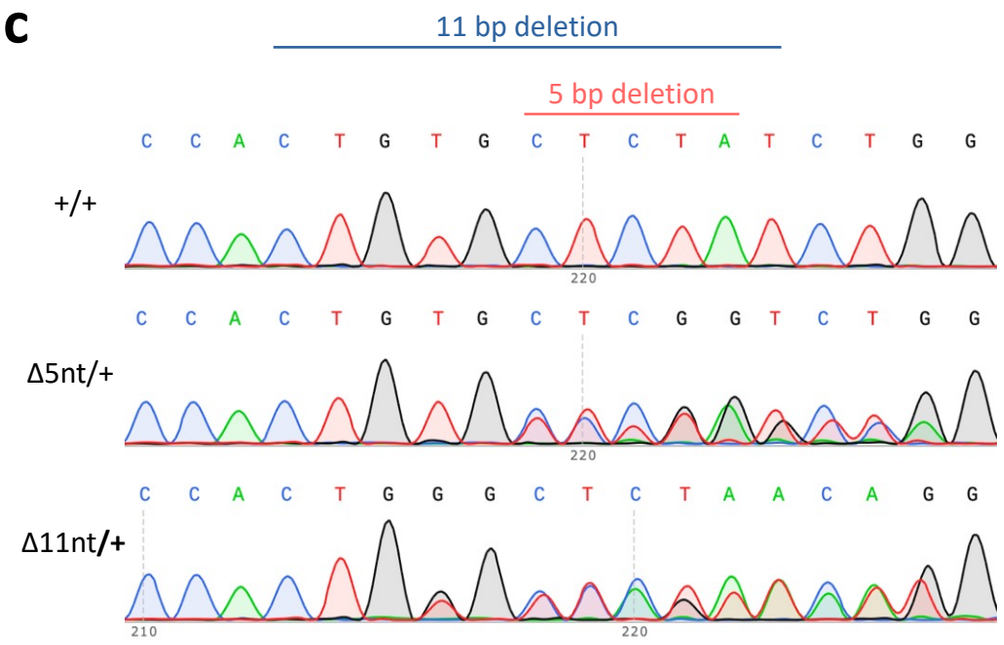

d

n	+/+	+/Δ	Δ/Δ	P value
48 hpf	24	49	16	0.3091
96 hpf	30	53	22	0.5410

e

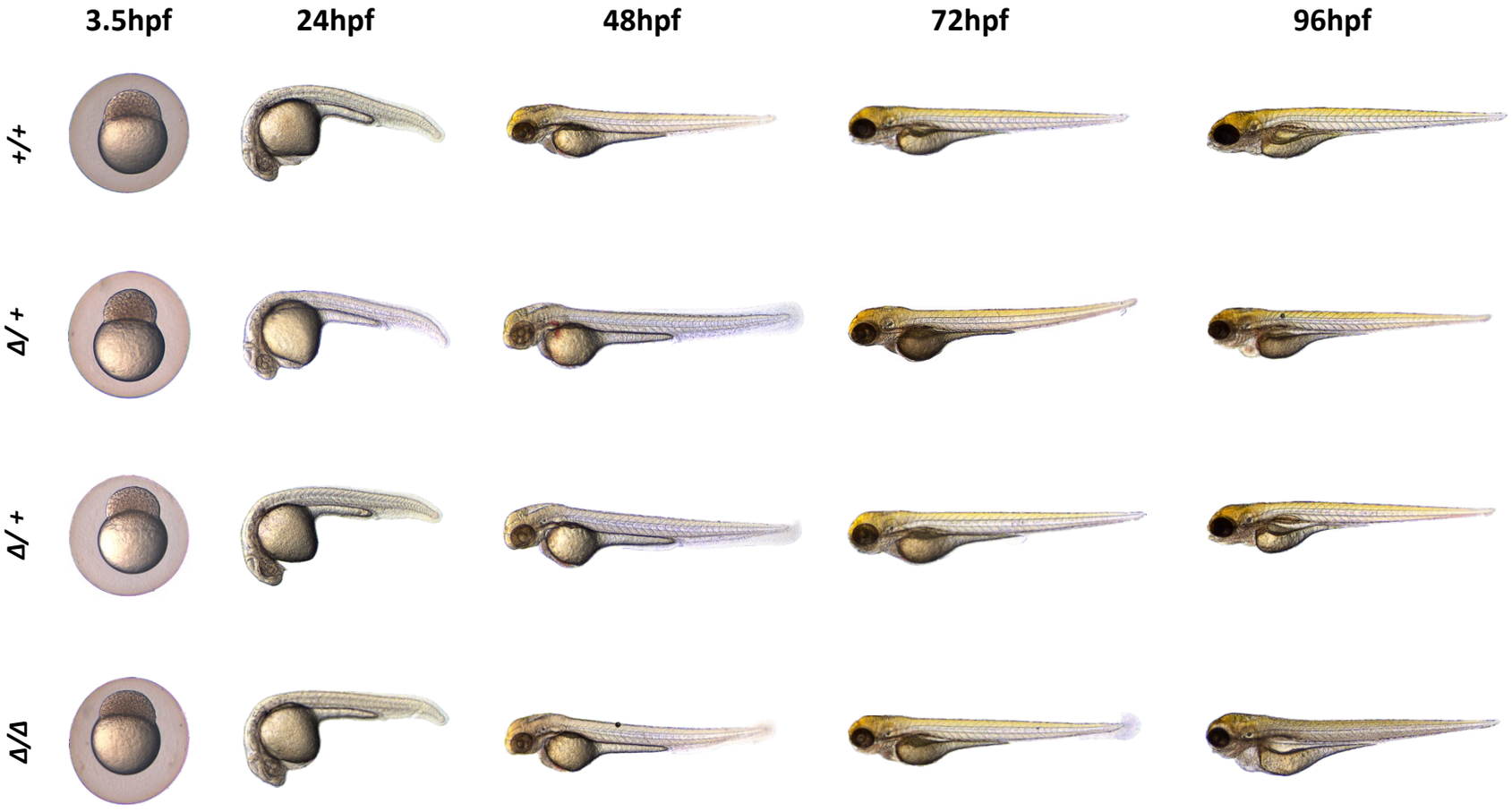

f

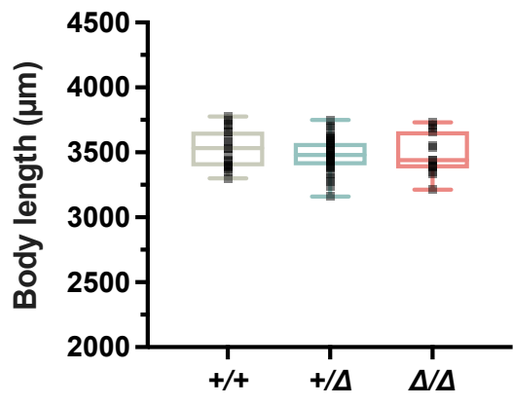

g

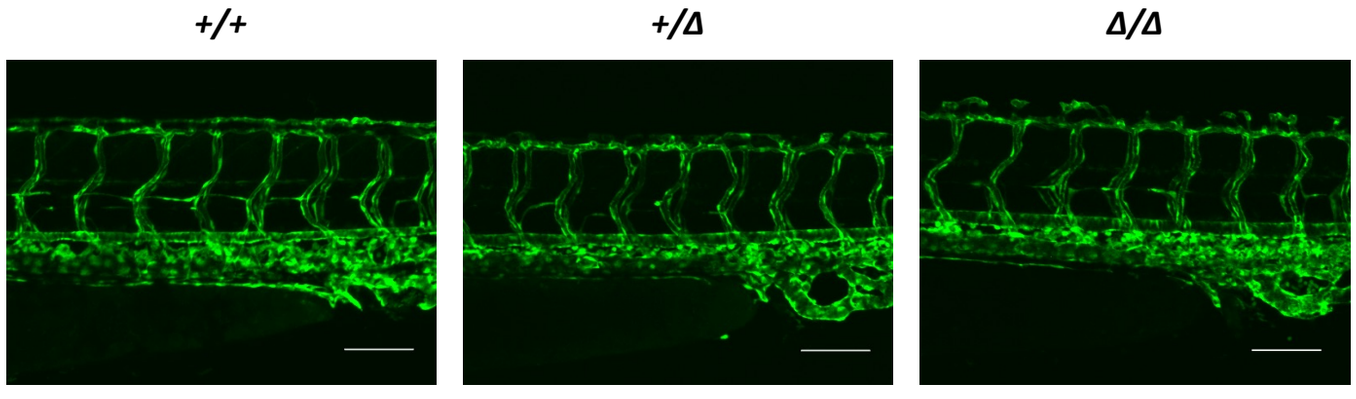

h

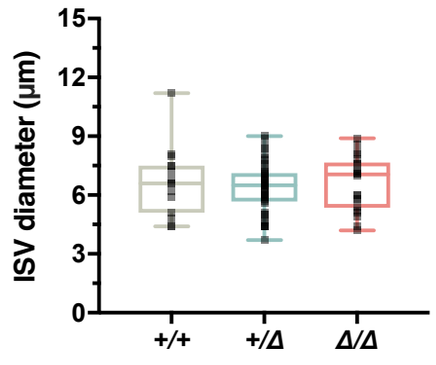

Figure S7. Developmental defects and cerebral vessel dysmorphism in tomm7-deleted zebrafish. (**a**) Targeted sequencing of *tomm7* in F1 zebrafish from backcross of F0 generation (obtained by the backcross of injected mosaic zebrafish to WT zebrafish) to WT zebrafish. Four representative frameshift mutations in *tomm7* were shown. (**b**) Targeted sequencing of *tomm7* in F0 zebrafish viewed with integrative genome viewer (IGV) showing heterozygous deletion of *tomm7*. (**c**) Confirmation of *tomm7*-deletions by Sanger sequencing. (**d**) Chi-square test of comparisons of observed ratios of +/+, +/Δ, and Δ/Δ F1 generation from the *tomm7*-deleted intercross with expected Mendelian ratio (25%, 50%, 25%) at 48 hpf and 96 hpf. Statistical analysis was performed using the chi-square goodness-of-fit test (**e**) Morphology of *tomm7*-deleted embryos from 3.5 hpf to 96 hpf. (**f**) Quantification of body length of *tomm7* zebrafish at 96 hpf. Statistical analysis was performed using Kruskal-Wallis test with Dunn's post hoc test for multiple comparisons. WT, N=19; *+*/Δ, N=34; Δ/Δ, N=14. (**g**) Representative images of intersegmental vessels (ISVs) in *Tg(fli1a: EGFP) tomm7* zebrafish at 48 hpf. Scale bars, 100 μm. (**h**) Quantification of ISV diameter in *tomm7* zebrafish at 48 hpf. The diameter of six ISVs from individual embryo was measured by ImageJ software. Statistical analysis was performed using Kruskal-Wallis test with Dunn's post hoc test for multiple comparisons. WT, N=2; +/Δ, N=6; Δ/Δ, N=3.

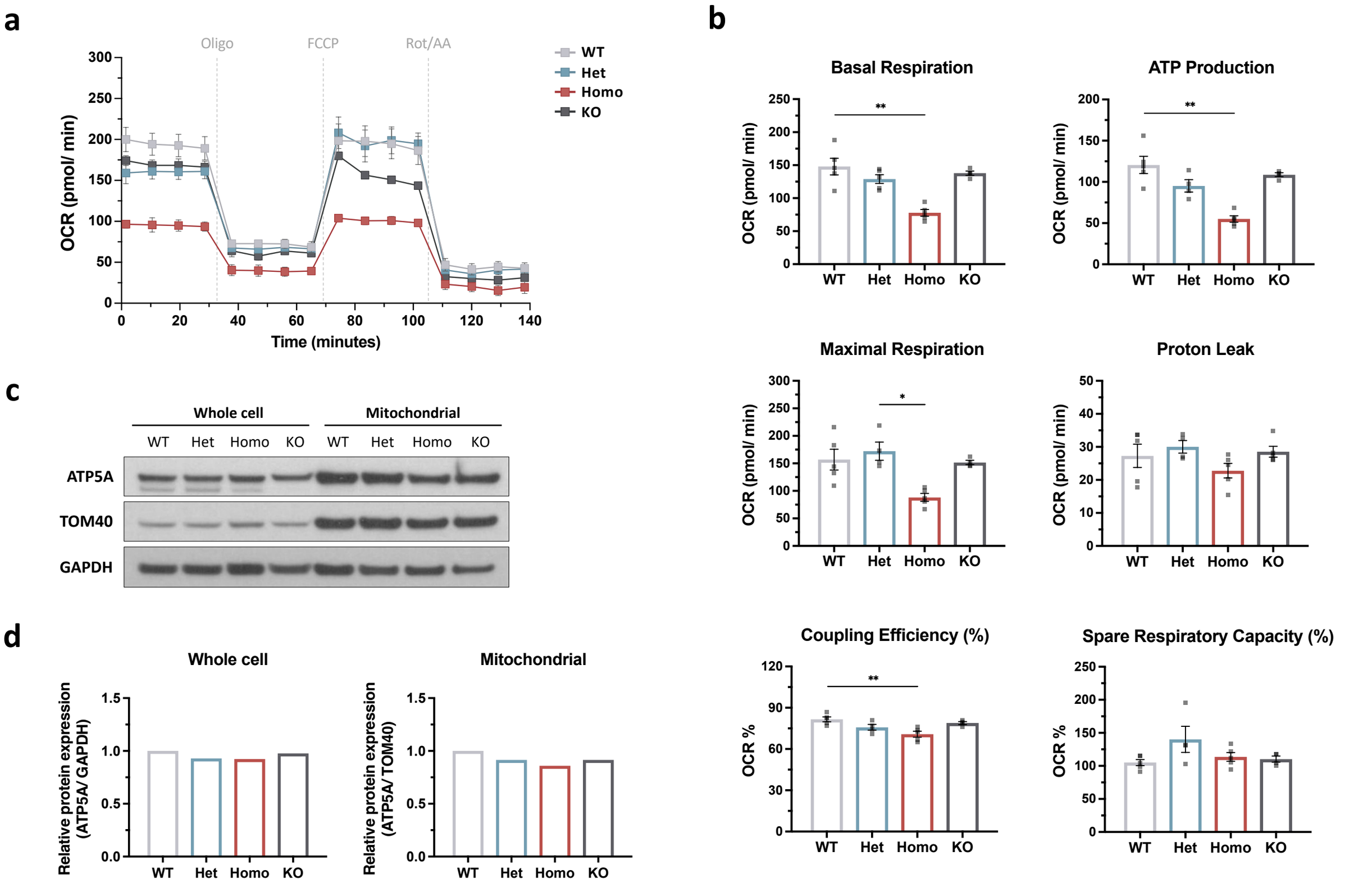

Figure S8. Mitochondrial respiration in iPSCs with *TOMM7* variant. (**a**) Representative oxygen consumption rate (OCR) analysis using the Seahorse Mito Stress Test with $3.5x10^4$ iPSCs. Oligo., oligomycin; FCCP, carbonyl cyanide-p-trifluoromethoxyphenylhydrazone; Rot, rotenone; AA, antimycin A. (**b**) Basal respiration, ATP-coupled respiration, maximal mitochondrial respiratory capacity, proton leak-linked respiration, percentage of respiration used for ATP synthesis, and spare respiratory capacity were calculated from the representative assay (a). Statistical analysis was performed using Kruskal-Wallis test with Dunn's multiple comparisons test. (**c**) Immunoblotting of differentially abundant protein components in whole-cell lysate and mitochondria-enriched lysates from iPSCs cells. (**d**) Quantitative analyses of the level of ATP5A in whole-cell or mitochondria-enriched lysates from (c). WT, wild-type; Het, heterozygous *TOMM7*$^{+/PL}$; Homo, homozygous *TOMM7*$^{PL/PL}$; KO, *TOMM7* knock-out. Data were presented as mean ± S.E.M. *P < 0.05, **P < 0.01, ***P < 0.001.

Figure S9. Transcriptome analysis in homozygous vs. heterozygous iPSCs. (**a**) Gene set enrichment analysis showing positively enriched Hallmark dataset in *TOMM7*$^{PL/PL}$ cells when compared with *TOMM7*$^{+/PL}$ cells. (**b**) Category network plot showing the linkage of significantly upregulated Hallmark gene sets in *TOMM7*$^{PL/PL}$ cells when compared with *TOMM7*$^{+/PL}$ cells. (**c**) Gene set enrichment analysis showing negative enriched GO terms in *TOMM7*$^{PL/PL}$ cells when compared with *TOMM7*$^{+/PL}$ cells. (**d**) Category network plot showing the linkage of significantly downregulated GO terms in *TOMM7*$^{PL/PL}$ cells when compared with *TOMM7*$^{+/PL}$ cells. (**e**) Dotplot showing the ratio of enriched genes in representing 11 significantly activated and suppressed GO terms in *TOMM7*$^{PL/PL}$ cells when compared with *TOMM7*$^{+/PL}$ cells. WT, wild-type; Het, heterozygous *TOMM7*$^{+/PL}$; Homo, homozygous *TOMM7*$^{PL/PL}$; KO, *TOMM7* knock-out.

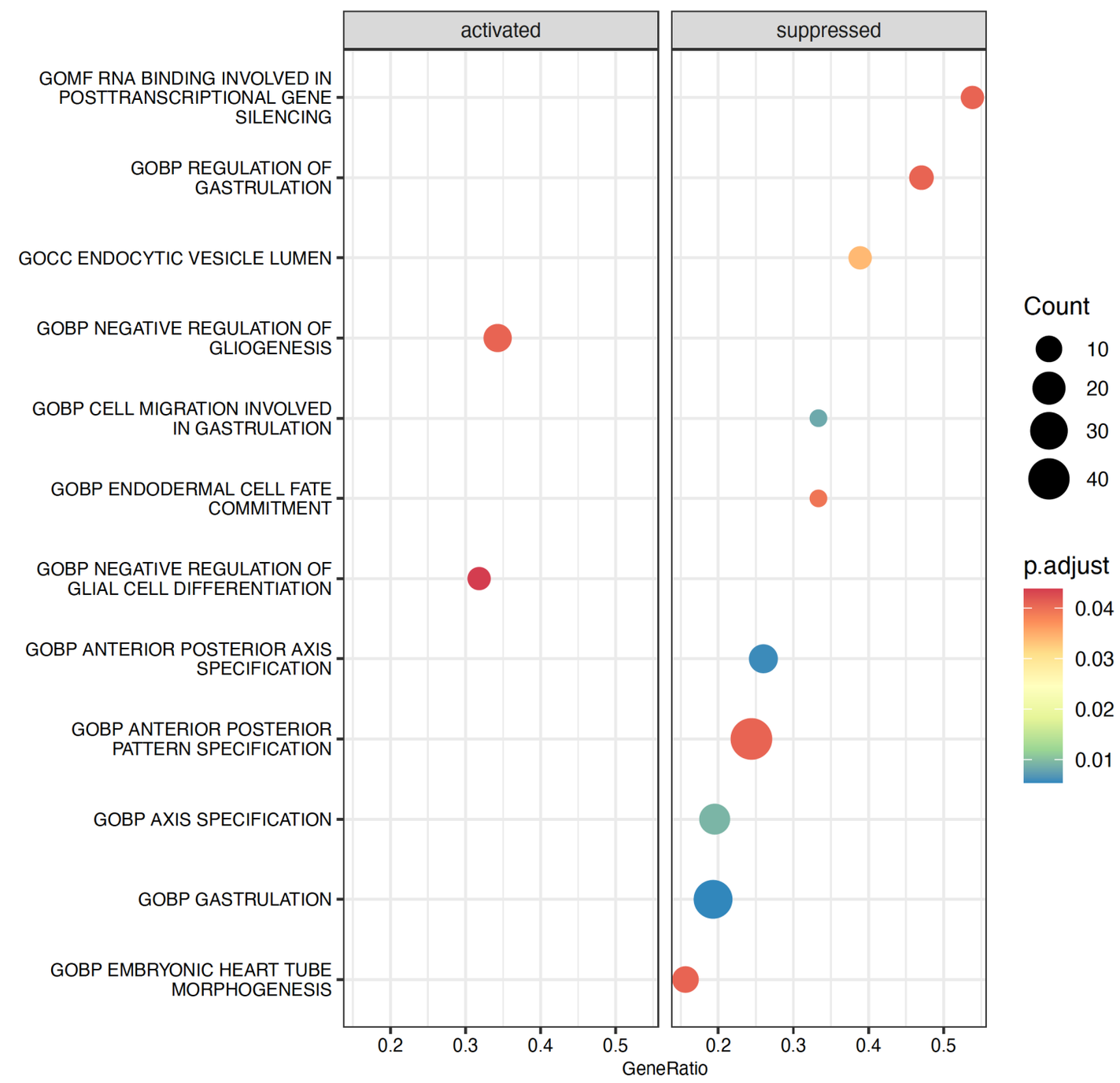

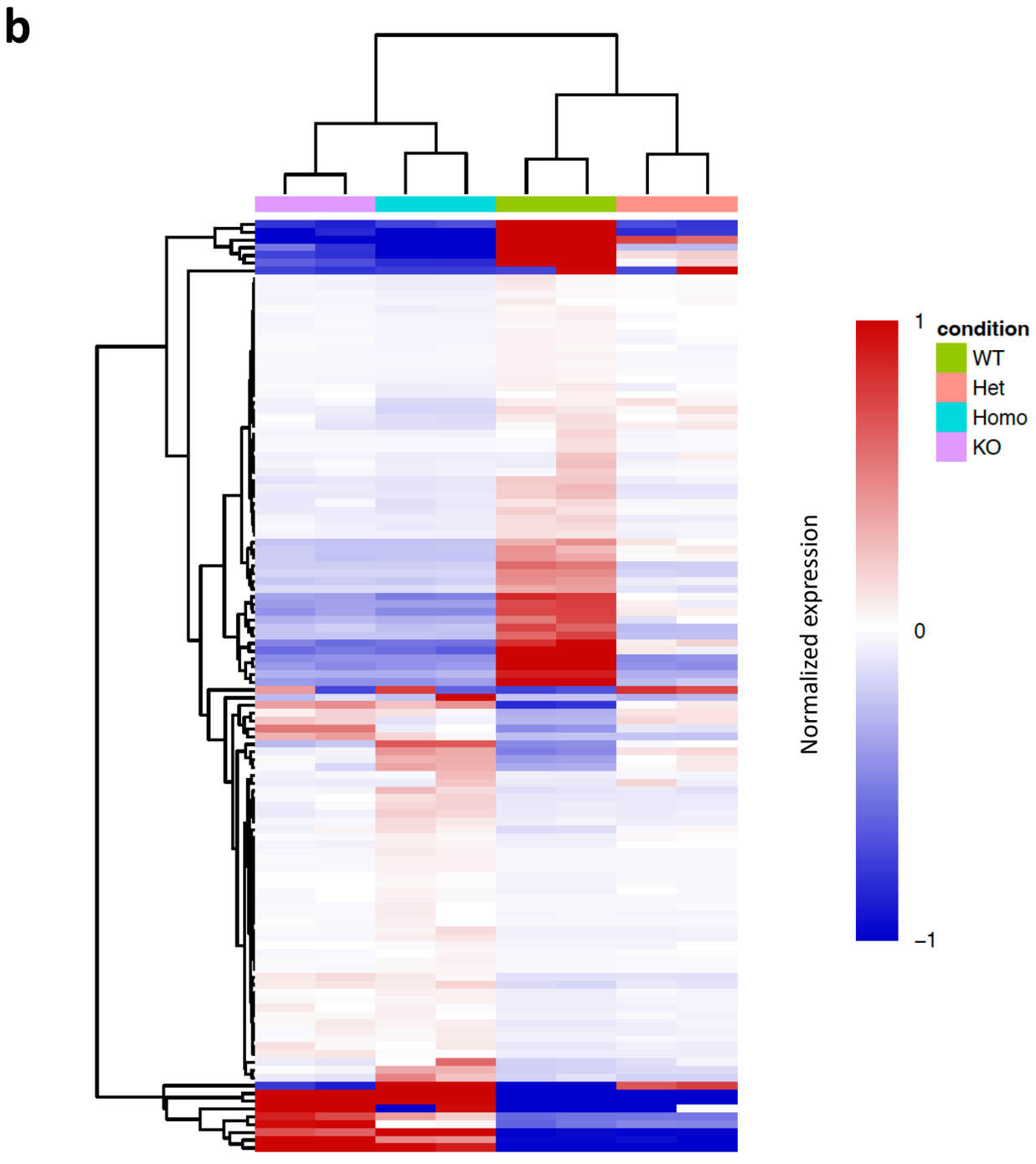

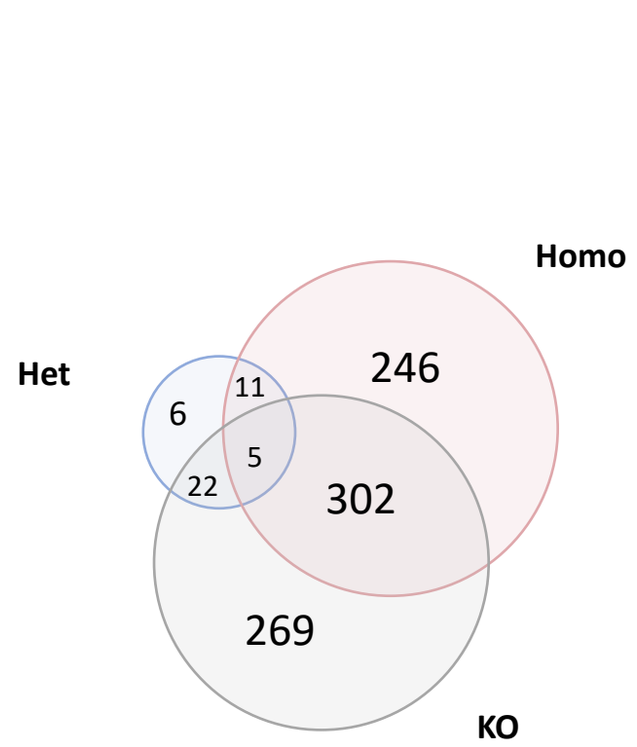

Figure S10. Transcriptome analysis in homozygous vs. WT iPSCs. (**a**) Dot plot showing the ratio of enriched genes in representing 12 significantly activated and suppressed GO terms in *TOMM7*$^{PL/PL}$ iPSCs when compared with WT cells. (**b**) Heatmap showing the unsupervised cluster of cell samples based on top 50 differentially expressed genes (identified by comparing *TOMM7*$^{PL/PL}$ with WT iEndo cells). (**c**) Venn diagram showing the number of shared or unique differentially expressed genes in iPSCs among *TOMM7* variants (when compared with WT). WT, wild-type; Het, heterozygous *TOMM7*$^{+/PL}$; Homo, homozygous *TOMM7*$^{PL/PL}$; KO, *TOMM7* knock-out *TOMM7*$^{-/-}$.

Figure S11. Transcriptome analysis in *TOMM7* knockout vs. WT iPSCs. (**a** and **b**) Gene set enrichment analyses showing significantly upregulated and downregulated Hallmark gene sets (a) and GO terms (b) in *TOMM7*$^{-/-}$ cells when compared with WT cells. (**c**) Category network plot showing the linkage of upregulated and downregulated genes and Hallmark datasets in *TOMM7*$^{-/-}$ cells when compared with WT cells. (**d**) Dotplot showing the ratio of enriched genes in representing 20 significantly activated or suppressed GO terms in *TOMM7*$^{-/-}$ cells when compared with WT cells. WT, wild-type; Het, heterozygous *TOMM7*$^{+/PL}$; Homo, homozygous *TOMM7*$^{PL/PL}$; KO, *TOMM7* knock-out, *TOMM7*$^{-/-}$.

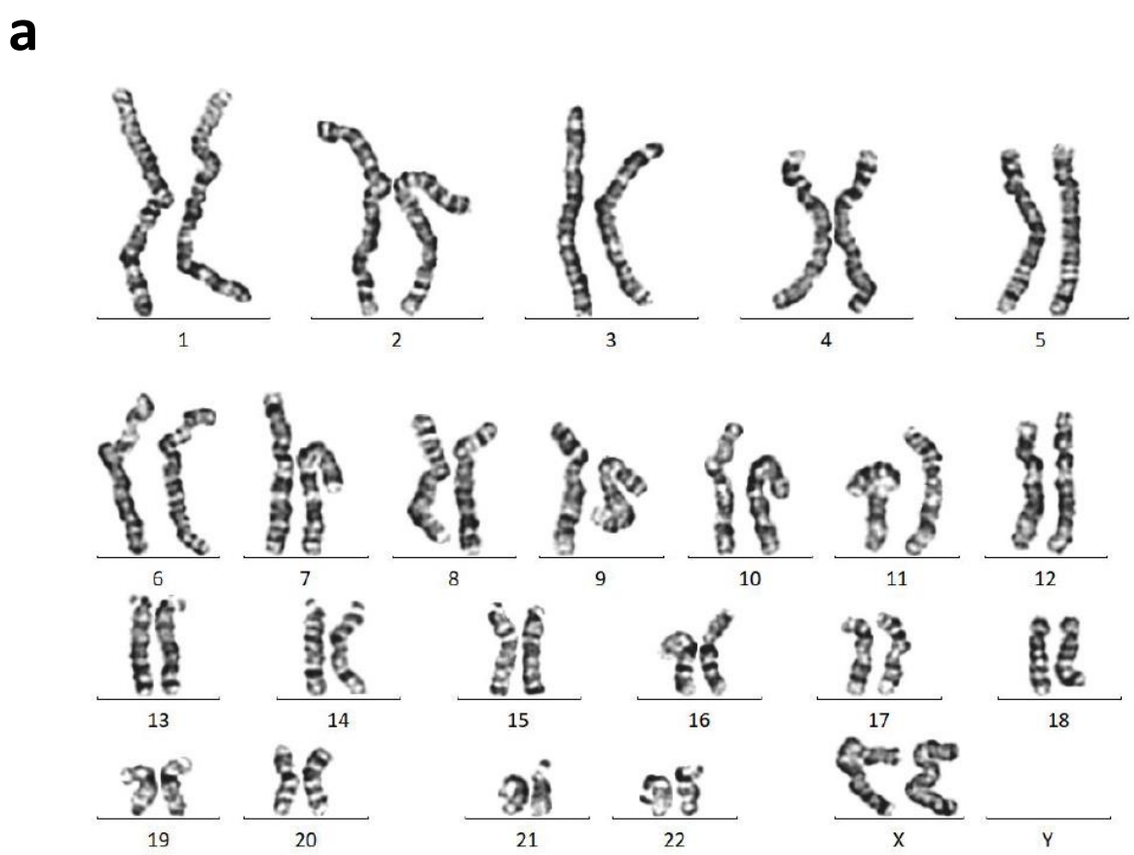

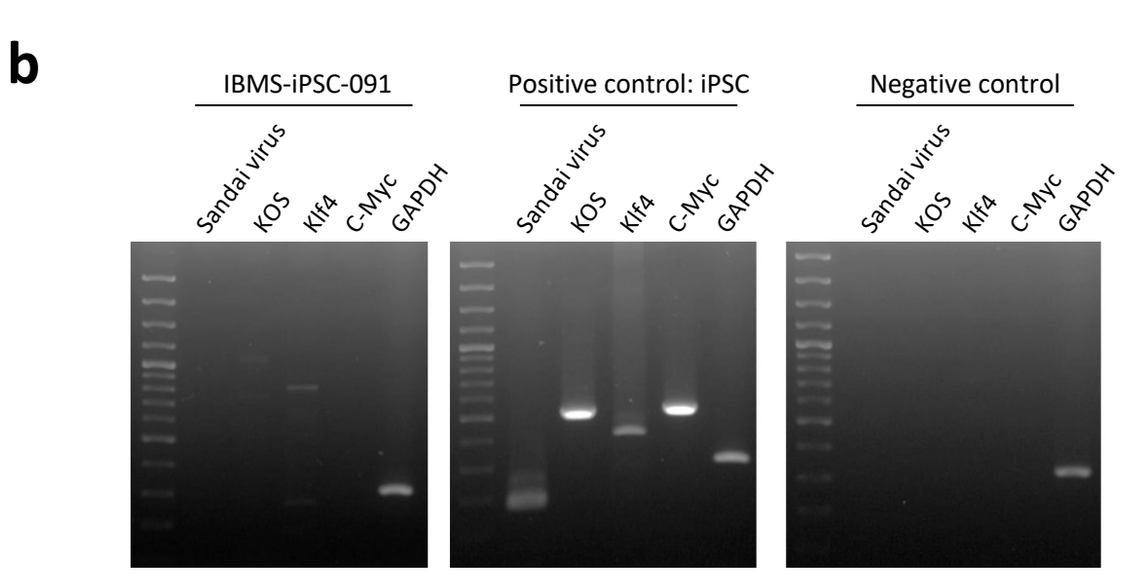

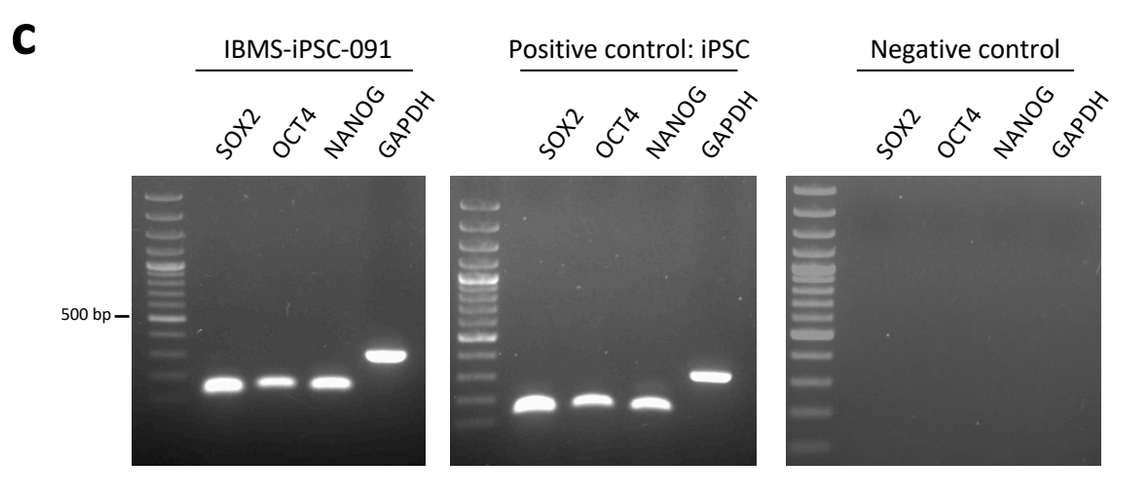

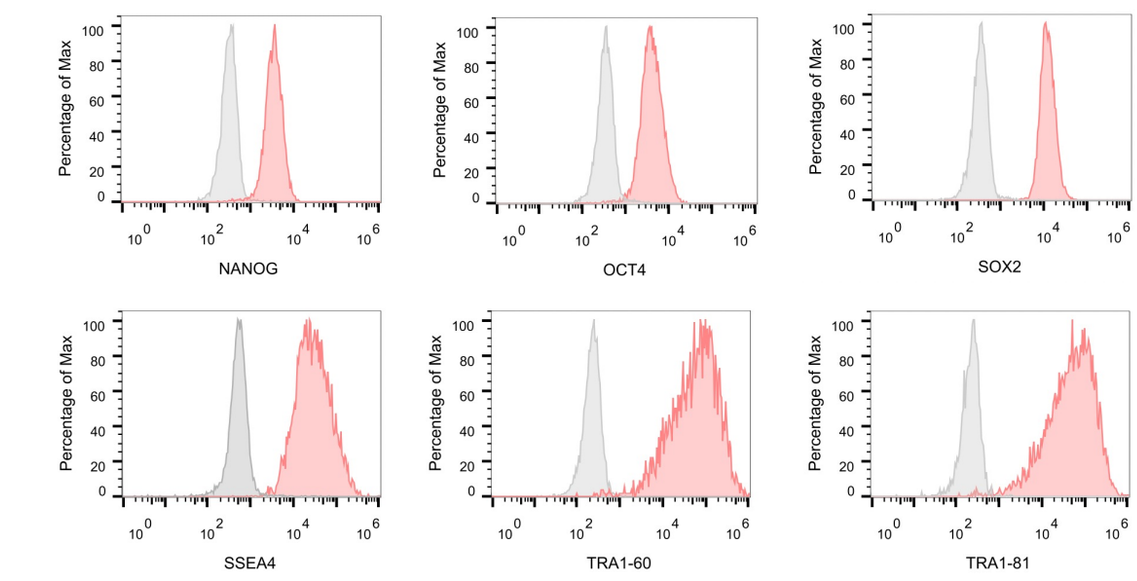

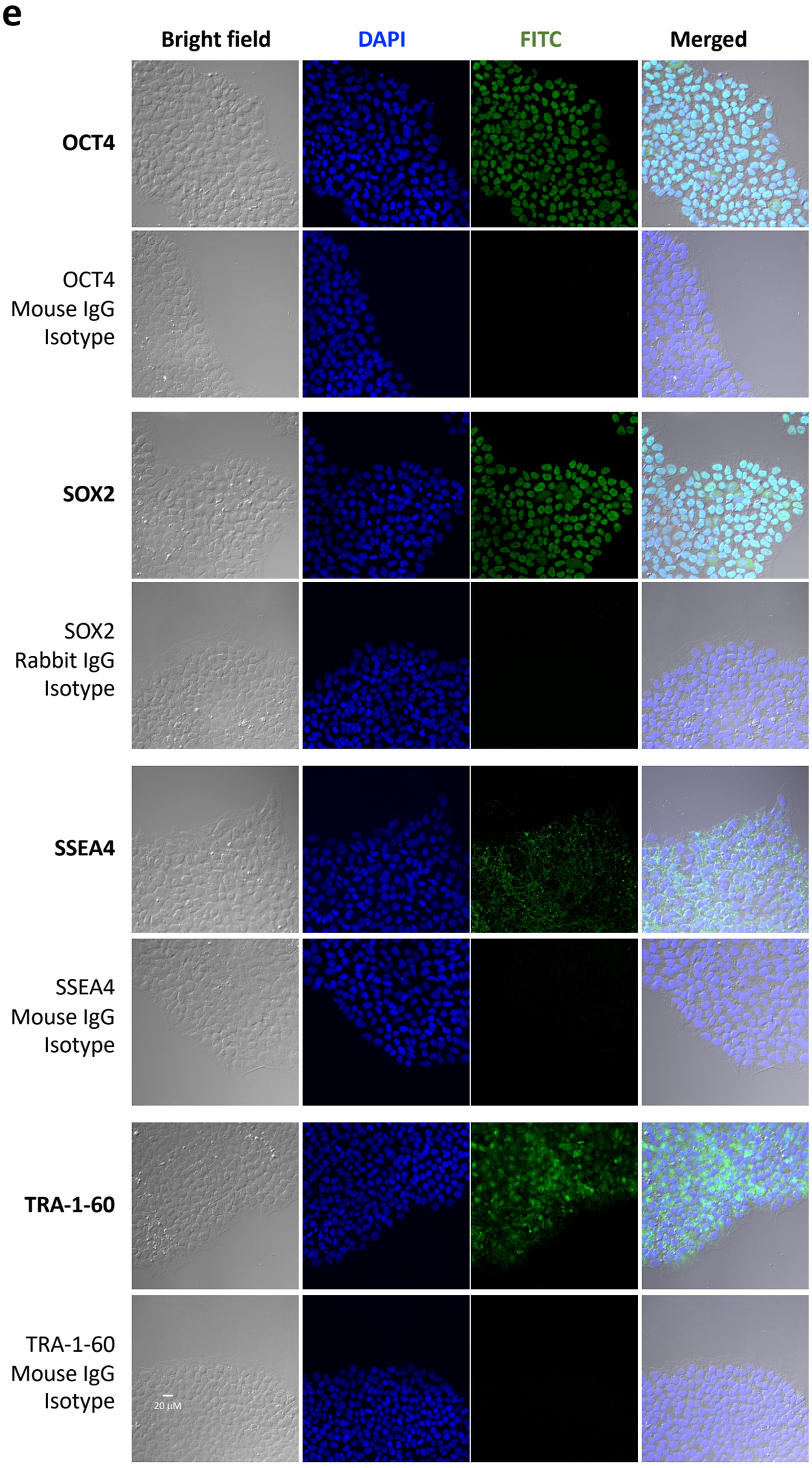

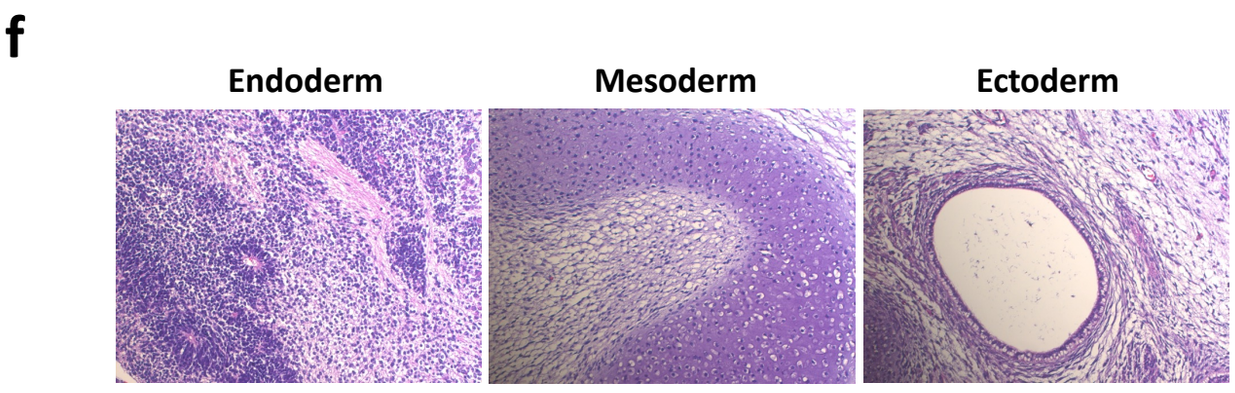

Figure S12. Reprogramming of iPSCs from patient 1-III's PBMCs. (**a**) Karyotyping with metaphase spreads of reprogrammed iPSCs at P12/P5 (P12 represented the total passage number, including 7 passages cultured in feeder-dependent and 5 more passages after shifting to the feeder-free cultivation). (**b**) Transgene-free confirmation was done with iPSCs at P8. (**c**) Pluripotency markers were evaluated by RT-PCR of reprogrammed iPSCs at P12/P5 with primers of Nanog, OCT4, and SOX2. (**d**) Pluripotency markers were evaluated in reprogrammed iPSCs at P12/P5 by flow cytometry of IBMS-iPSC-091-01 P16/P9 with SSEA4, TRA-1-60, TRA-1-81, OCT4, SOX2, and Nanog (**e**) Pluripotency markers were evaluated by immunochemistry in reprogrammed iPSCs at P12/P5 staining with SSEA4, SOX2, TRA-1-60 and OCT4. (**f**) Teratoma formation with reprogrammed iPSCs (P12/P5) injected into 8 weeks old NOD/SCID mice's testes were harvested 8 weeks later and stained with Hematoxylin and Eosin stain.

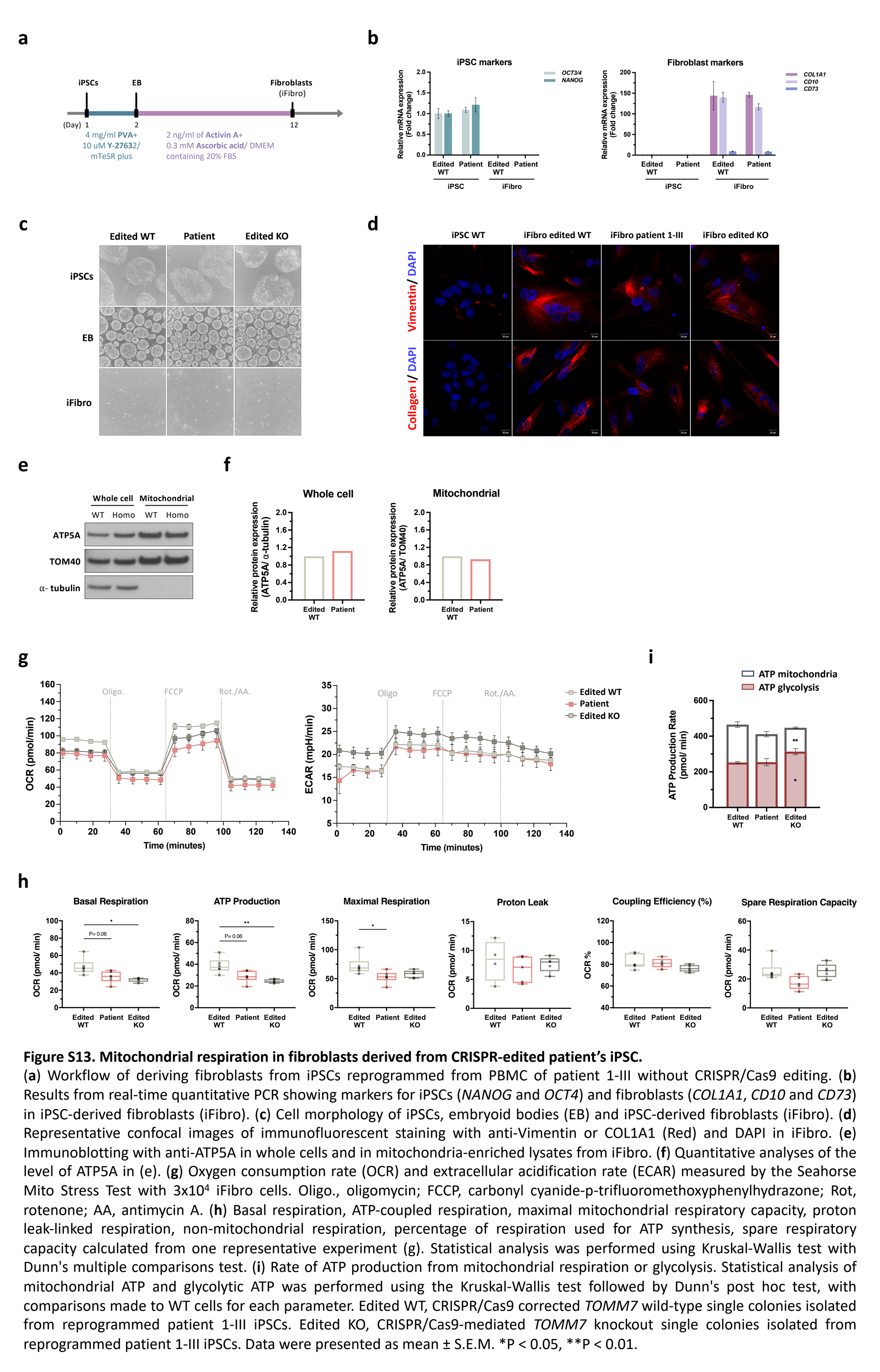

Figure S13. Mitochondrial respiration in fibroblasts derived from CRISPR-edited patient's iPSC.

(**a**) Workflow of deriving fibroblasts from iPSCs reprogrammed from PBMC of patient 1-III without CRISPR/Cas9 editing. (**b**) Results from real-time quantitative PCR showing markers for iPSCs (*NANOG* and *OCT4*) and fibroblasts (*COL1A1*, *CD10* and *CD73*) in iPSC-derived fibroblasts (iFibro). (**c**) Cell morphology of iPSCs, embryoid bodies (EB) and iPSC-derived fibroblasts (iFibro). (**d**) Representative confocal images of immunofluorescent staining with anti-Vimentin or COL1A1 (Red) and DAPI in iFibro. (**e**) Immunoblotting with anti-ATP5A in whole cells and in mitochondria-enriched lysates from iFibro. (**f**) Quantitative analyses of the level of ATP5A in (e). (**g**) Oxygen consumption rate (OCR) and extracellular acidification rate (ECAR) measured by the Seahorse Mito Stress Test with $3x10^4$ iFibro cells. Oligo., oligomycin; FCCP, carbonyl cyanide-p-trifluoromethoxyphenylhydrazone; Rot, rotenone; AA, antimycin A. (**h**) Basal respiration, ATP-coupled respiration, maximal mitochondrial respiratory capacity, proton leak-linked respiration, non-mitochondrial respiration, percentage of respiration used for ATP synthesis, spare respiratory capacity calculated from one representative experiment (g). Statistical analysis was performed using Kruskal-Wallis test with Dunn's multiple comparisons test. (**i**) Rate of ATP production from mitochondrial respiration or glycolysis. Statistical analysis of mitochondrial ATP and glycolytic ATP was performed using the Kruskal-Wallis test followed by Dunn's post hoc test, with comparisons made to WT cells for each parameter. Edited WT, CRISPR/Cas9 corrected *TOMM7* wild-type single colonies isolated from reprogrammed patient 1-III iPSCs. Edited KO, CRISPR/Cas9-mediated *TOMM7* knockout single colonies isolated from reprogrammed patient 1-III iPSCs. Data were presented as mean ± S.E.M. *P < 0.05, **P < 0.01.